

# Resolving the Molecular Origin of Mechanical Relaxations in Donor-Acceptor Polymer Semiconductors

Nrup Balar, Jeromy James Rech, Salma Siddika, Runqiao Song, Harry M. Schrickx, Nadeem Sheikh, Long Ye, Anthony Megret Bonilla, Omar Awartani, Harald Ade, Wei You,\* and Brendan T. O'Connor\*

The thermomechanical behavior of polymer semiconductors plays an important role in the processing, morphology, and stability of organic electronic devices. However, donor-acceptor-based copolymers exhibit complex thermal relaxation behavior that is not well understood. This study uses dynamic mechanical analysis (DMA) to probe thermal relaxations of a systematic set of polymers based around the benzodithiophene (BDT) moiety. The loss tangent curves are resolved by fitting Gaussian functions to assign and distinguish different relaxations. Three prominent transitions are observed that correspond to: i) localized relaxations driven primarily by the side chains  $(\gamma)$ , ii) relaxations along the polymer backbone  $(\beta)$ , and iii) relaxations associated with aggregates ( $\alpha$ ). The side chains are found to play a clear role in dictating  $T_n$  and that mixing the side chain chemistry of the monomer to include alkyl and oligo(ethylene glycol) moieties results in splitting the  $\gamma$ -relaxation. The  $\beta$  relaxations are shown to be associated with backbone elements along with the monomer. In addition, through processing, it is shown that the  $\alpha$ -relaxation is due to aggregate formation. Finally, it is demonstrated that the thermal relaxation behavior correlates well with the stress-strain behavior of the polymers, including hysteresis and permanent set in cyclically stretched films.

1. Introduction

The thermomechanical behavior of commodity polymers has been widely studied to understand the origin of a range of properties including fracture toughness, elasticity, creep, thermal stability, and diffusion.<sup>[1,2]</sup> Many of these properties are also critically important in polymer semiconductors that are used in organic electronic devices. The thermal behavior impacts

not only the expected mechanical properties,<sup>[3–5]</sup> but also the microstructural evolution during processing, morphological stability,<sup>[6]</sup> and temperature stability.<sup>[7,8]</sup> As the performance of organic electronics continues to improve, it is becoming increasingly important that their thermomechanical properties are captured fully and the observed behavior is related back to molecular structure.

Current high-performance polymer semiconductors typically consist of alternating electron-donating and electron-accepting moieties (referred to as D–A copolymers) that allow for tuning key optoelectronic properties such as bandgap and energy levels. [9–11] In addition, these polymers typically have large side chains that allow solution processability. The relatively large and complex monomer structure of D–A copolymers leads to complex thermomechanical behavior. [12–14] In addition, the relatively rigid backbone and ordered packing also lead to small enthalpic changes upon relaxations

(i.e., small changes in heat capacity) making them difficult to observe using commonly used differential scanning calorimetry (DSC). The combination of complex and weak relaxation signatures of these organic semiconductors has made it a challenge to correlate thermomechanical behavior to chemical structure. Nevertheless, progress has been made including several recent studies that have probed the thermal relaxation of D–A copolymers by varying the polymer structures.<sup>[5,15–17]</sup> Among these,

N. Balar, R. Song, H. M. Schrickx, N. Sheikh, B. T. O'Connor Department of Mechanical and Aerospace Engineering and Organic and Carbon Electronics Laboratories (ORaCEL) North Carolina State University Raleigh, NC 27695, USA E-mail: btoconno@ncsu.edu

J. J. Rech, A. Megret Bonilla, W. You Department of Chemistry University of North Carolina Chapel Hill, NC 27599, USA E-mail: wyou@unc.edu

The ORCID identification number(s) for the author(s) of this article can be found under https://doi.org/10.1002/adfm.202105597.

DOI: 10.1002/adfm.202105597

S. Siddika

Department of Materials Science and Engineering and Organic and Carbon Electronics Laboratories (ORaCEL) North Carolina State University Raleigh, NC 27695, USA

L. Ye, H. Ade
Department of Physics
and Organic and Carbon Electronics Laboratories (ORaCEL)
North Carolina State University
Raleigh, NC 27695, USA
O. Awartani

Department of Mechanical Engineering
Maroun Semaan Faculty of Engineering and Architecture
American University of Beirut
Beirut 1107-2020, Lebanon



\_\_\_\_MATERIALS
www.afm-iournal.de

thermal relaxations in a series of molecular weights (MWs) of PBnDT-FTAZ were studied by Balar et al.;<sup>[15]</sup> Zhang et al. investigated the impact of side-chain and backbone modifications in the DPP based copolymers;<sup>[17]</sup> Balar et al.<sup>[5]</sup> and Sharma et al.<sup>[16]</sup> explored the role of molecular structures across a broad variety of polymer semiconductors. Yet, the studies focused on probing the dominant thermal relaxation limiting the understanding of the origin of the multiple relaxations often observed.[15,17-19] A model has also recently been introduced that applies an effective molecular mobility to elements of the monomer to predict the glass transition temperature  $(T_g)$  in conjugated polymers.<sup>[20]</sup> While this model was shown to work well in a number of polymers, it is not universally applicable as illustrated in Table S1 (Supporting Information). [21,22] This is complicated by the fact that the most prominent or the highest temperature relaxation observed has been designated as the  $T_g$  in the literature.<sup>[17,19,23]</sup> Yet, these relaxations do not always show the behavior of a classically defined glass transition where the mechanical relaxation corresponds to the coordinated motion of several monomers or more. [24,25] For example, the relaxations in D-A copolymers do not always show an MW dependence, a large drop in storage modulus (E') in the largely amorphous polymers, or change in optical properties that one would expect for a glass transition. [15,17,26] Alternatively, the observed mechanical relaxations may be localized in nature, often referred to as secondary or  $sub-T_g$  relaxations.<sup>[5,16]</sup> Some reports have asserted that the prominent relaxation observed in many D-A copolymers is indeed a local relaxation. [5,16] Thus, there remain contradictions on designating a thermal relaxation as a  $T_{\alpha}$  and continued ambiguity associated with the molecular origin of the multiple relaxations often observed with dynamic mechanical analysis (DMA) and rheology.

In this article, we provide clear evidence that relates the observed thermal relaxations to specific molecular and morphological features of D-A copolymers. We focus on characterizing the thermomechanical behavior of benzodithiophene (BDT) based D-A copolymers (Figure 1). BDT-based polymers have been widely employed in high-performance D-A copolymer derivatives that have demonstrated high charge mobilities<sup>[27]</sup> and high solar cell power conversion efficiency.<sup>[28–31]</sup> For example, the current record efficiency solar cell employs D18 that has a functionalized BDT donor moiety.[10] We applied DMA to study the thermal transitions in a systematic set of polymers as DMA is significantly more sensitive than commonly used DSC,[18,32,33] providing deeper insight into the relaxation behavior. We first introduce the thermal transitions observed by considering the base polymer, PBnDT-FTAZ with the molecular structure shown in Figure 1a. We then systematically vary elements along the backbone (PBnDT, noT-FTAZ), followed by side-chain substitution with alkyl (PBnODT-FTAZ, PBnDTT-FTAZ) and oligo(ethylene glycol) (OEG) side chains (PBoDT-FTAZ, PBnDT-FTAZ<sub>NO</sub>, PBoDT- $FTAZ_{NO}$ , PBnDT-OTAZ, PBoDT-OTAZ) and finally changes to the amount of fluorination along the backbone (PBnDT-HTAZ, 4FT-HTAZ, 4FT-FTAZ), as shown in Figure 1. We also introduce the use of Gaussian functions to fit the loss tangent (tan  $\delta = E''/E'$  where E'' is the loss modulus) of the polymers to gain insight into the molecular origin of the relaxation behavior. The relationship of the thermal relaxation with the viscoelastic-plastic behavior of selected polymers under large cyclic strain is then discussed.

Through this systematic investigation, we are able to identify several key molecular features that drive the multiple mechanical relaxations observed through DMA. We find that despite large differences in the chemical structure of the polymers, we see similar relaxation temperatures attributed to the dominance of the side chain relaxation and common relaxation mechanisms along the conjugated backbone. We find that the side-chains play a dominant role in not only the relaxation temperature but also the extent of mechanical relaxation. Furthermore, through varying the processing conditions of the samples, we are able to clearly show that the high-temperature relaxations often observed in D-A copolymers are associated with ordered aggregates, and none of the studied polymers exhibit a clear glass transition. Finally, we demonstrate that the relaxation behavior also impacts the stress-strain behavior of the polymers with implications for flexible and stretchable devices.

### 2. Results and Discussion

#### 2.1. Approach

Figure 1 presents the molecular structures of the polymers considered and are grouped based on modifications to the base polymer PBnDT-FTAZ (with synthesis details provided in the Supporting Information). The base polymer has a BDT donor and benzotriazole (TAZ) acceptor moiety separated by thiophene linkers. The TAZ moiety is also fluorinated (FTAZ), which has been shown to modify the energy levels and improve packing order.[28,34,35] While PBnDT-FTAZ forms well-ordered aggregates (or paracrystallites), the films have been found to be largely amorphous.<sup>[15]</sup> The polymers considered are categorized into four groups in Figure 1 by systematic structural changes. i) The polymer backbone was varied by synthesizing a polymer with solely the BnDT moiety (PBnDT), and BnDT linked to the FTAZ moiety sans the thiophene linkers (noT-FTAZ). ii) The side chains on the BDT moiety were varied from having branched alkyl (3-butylnonyl) to alkoxy (PBnODT-FTAZ) and alkyl thiophene (PBnDTT-FTAZ) side chains. The branched alkyl side chains on the BDT moiety were also replaced with OEG side chains (PBoDT-FTAZ). iii) The addition of OEG side-chains on the TAZ moiety was then considered, replacing the alkyl side-chain (PBnDT-FTAZ<sub>NO</sub>, PBoDT-FTAZ<sub>NO</sub>), and placing OEG side-chains on the TAZ moiety at the previously fluorinated sites (PBnDT-OTAZ, PBoDT-OTAZ).[36] Lastly, iv) fluorination along the backbone was varied including the fluorination of the TAZ moiety (PBnDT-HTAZ and PBnDT-FTAZ) and fluorination of the thiophene linkers (4FT-HTAZ, 4FT-FTAZ). [37,38] Overall, we consider 13 unique variants of the BDT-TAZ based D-A copolymer and use consistent processing across all polymers to limit process-dependent variability. These polymers are amorphous similar to FTAZ, with the exception of PBnDT which is semicrystalline indicated by DSC scans given in Figure S14 (Supporting Information).

Thermal relaxation in polymers is commonly explained using the crankshaft model as shown schematically for PBnDT-FTAZ

### (a) Building Blocks

$$\begin{array}{c} C_4 H_9 \\ C_6 H_{13} \\ C_6 H_{13} \\ C_6 H_{13} \\ C_4 H_9 \\ \hline \\ C_6 H_{13} \\ C_4 H_9 \\ \hline \\ PBnDT-FTAZ \\ \end{array}$$

### (b) BnDT Side-chains

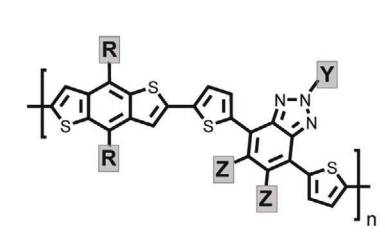
$$\mathbf{R} = \sum_{\mathbf{C_4} \mathbf{H_q}}^{\mathbf{S}} \mathbf{C_2}^{\mathbf{H_q}}$$

$$R = C_{6}^{H_{11}}$$

PBoDT-FTAZ

$$R = \sqrt{0}$$

### (c) Ethylene Glycol Side-chains



PBoDT-FTAZ<sub>NO</sub> 
$$\mathbf{R} = \sqrt{2}$$

$$R = C_6^{C_6H}$$

PBoDT-OTAZ

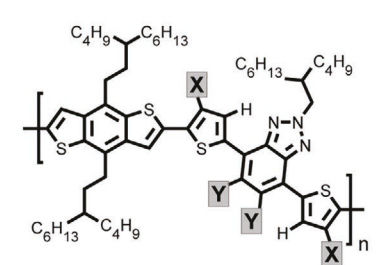
$$R = \sqrt{0}$$

PBnDT-OTAZ

$$\mathbf{R} = \frac{\mathbf{C}_{6} \mathbf{H}_{1}}{\mathbf{C}_{1} \mathbf{H}_{2}}$$

$$Y = \begin{array}{c} C_6 H_{13} \\ C_4 H_0 \end{array}$$

### (d) Fluorination



**PBnDT-HTAZ** 

X = H

Y = H

4FT-HTAZ

X = F

Y = H

4FT-FTAZ

X = FY = F

Figure 1. Molecular structures of the polymers studied.

in Figure 2a.<sup>[25]</sup> The relaxations of the side-chains typically occur at the lowest temperature and are due to the conformal changes in the C-C-C bonds.[39] Additional relaxation along the polymer backbone then occurs through a combination of relaxation of individual moieties along the backbone followed by coordinated relaxation of the several backbone moieties, then coordinated movement of several monomers (typically ascribed as the glass transition). Finally, larger-scale relaxation of aggregates or rigid amorphous phase may occur.<sup>[5,16,40]</sup> We will use this crankshaft model perspective when correlating the molecular structure to the observed relaxation behavior in the systematically varied polymers.

www.advancedsciencenews.com www.afm-journal.de

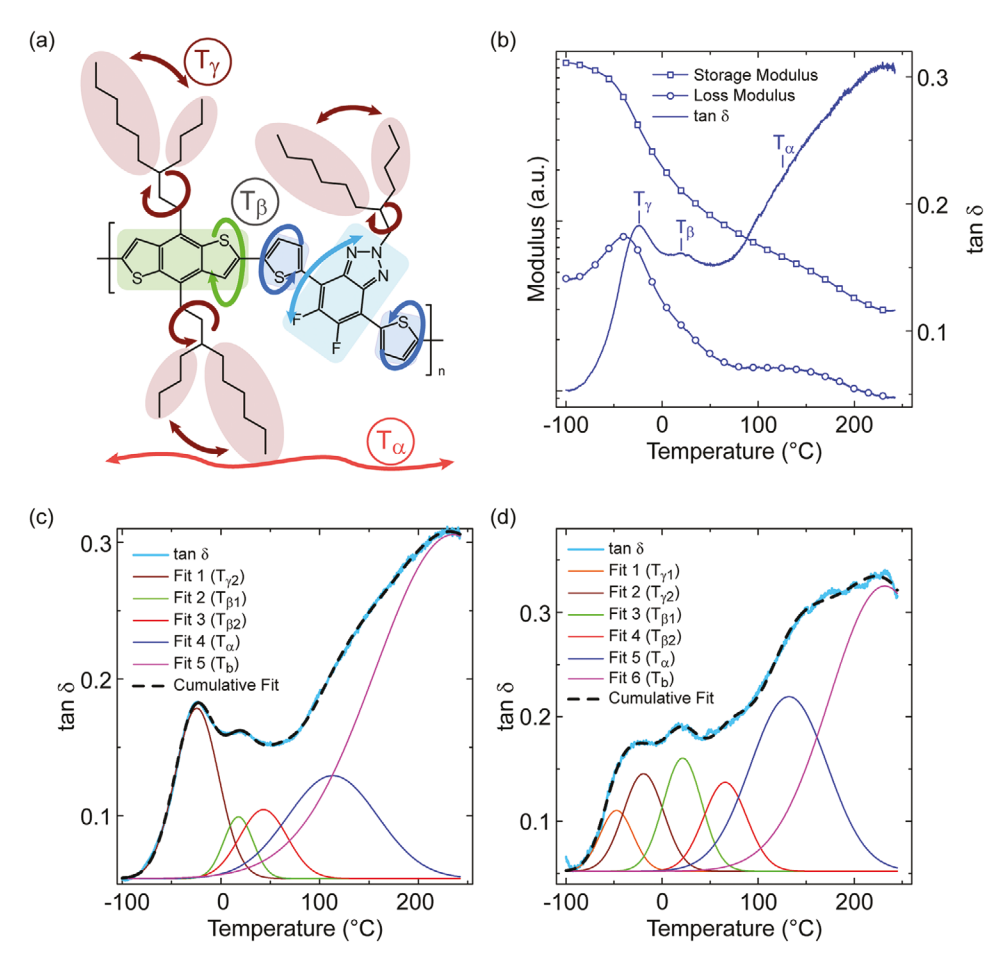


Figure 2. a) Schematic of possible molecular motions in PBnDT-FTAZ based on a crankshaft model and b) the DMA scan of PBnDT-FTAZ at the oscillation frequency of 1 Hz and the temperature ramp of 3 °C min<sup>-1</sup>. Gaussian peak fitted tan  $\delta$  versus temperature curves of the variants with c) a single  $\gamma$ -transition peak (PBnDT-FTAZ) and d) a split  $\gamma$ -transition peak (PBnDT-FTAZ). The  $\gamma$ -transition peaks of the polymers that are fitted with only one Gaussian function are denoted as  $\gamma$ 2.

We first consider the base polymer PBnDT-FTAZ, where three primary thermal relaxations are identified from the peaks in tan  $\delta$ , as shown in Figure 2b. The highest temperature transition is indicated as  $T_{\alpha}$  (127 °C) followed by  $T_{\beta}$ (19 °C), and  $T_{\gamma}$  (–23 °C) in the order of decreasing temperature. To gain further insight into the relaxation behavior, we fit the tan  $\delta$  curve with a series of Gaussian functions, as shown in Figure 2c. The Gaussian distributions represent the relaxation of a molecular or microstructural feature in the polymer.[41,42] Here, it can be seen that a minimum of five Gaussian functions can accurately reproduce the entire tan  $\delta$  curve. The Gaussian fit procedure is described in detail in Supporting Information. The lowest temperature Gaussian accurately captures  $T_r$  The  $\beta$ -relaxation peak, on the other hand, exhibits an asymmetric shape requiring two Gaussian functions to accurately reflect the experimental data, and is indicative of multiple relaxation processes. The fourth Gaussian captures  $T_{op}$ which we attribute to the relaxation of aggregates as discussed below. The fifth Gaussian function is a bit more ambiguous and could represent an additional relaxation, lengthening of the sample resulting in a relaxation signature, or other background relaxation of the system during the test.[16,42] Thus, we

label this last Gaussian function peak temperature as  $T_{\rm b}$ . The exception being PBnDT which exhibits melting at ≈110 °C as shown by DSC (Figure S14a, Supporting Information). We will use the Gaussian fits of tan  $\delta$  and related peak temperatures  $(T_{\gamma 1}, T_{\gamma 2}, T_{\beta 1}, T_{\beta 2}, T_{\alpha 1}, T_{\rm b})$  to discuss the differences in relaxation behavior. Here, a ytransition temperature is denoted as  $T_{\mathcal{D}}$  if the peak could be fitted with just one Gaussian function. While the Gaussian peak temperatures may vary from the peaks observed in the raw tan  $\delta$  curve, they provide a systematic and quantitative approach to distinguish the thermomechanical behavior of the polymers. A comparison of tan  $\delta$ organized by polymer grouping is given in Figure 3 (with the storage modulus and loss modulus given in Figures S15-S19, Supporting Information). The Gaussian fits to tan  $\delta$  for each polymer are given in Figures S26-S32 (Supporting Information) and the peak temperatures are provided in Table 1.

### 2.2. The Local Nature of the $\gamma$ - and $\beta$ -Relaxations

The thermomechanical behavior of D–A copolymers is complex, and we do not attempt to explain all nuances. Nevertheless,

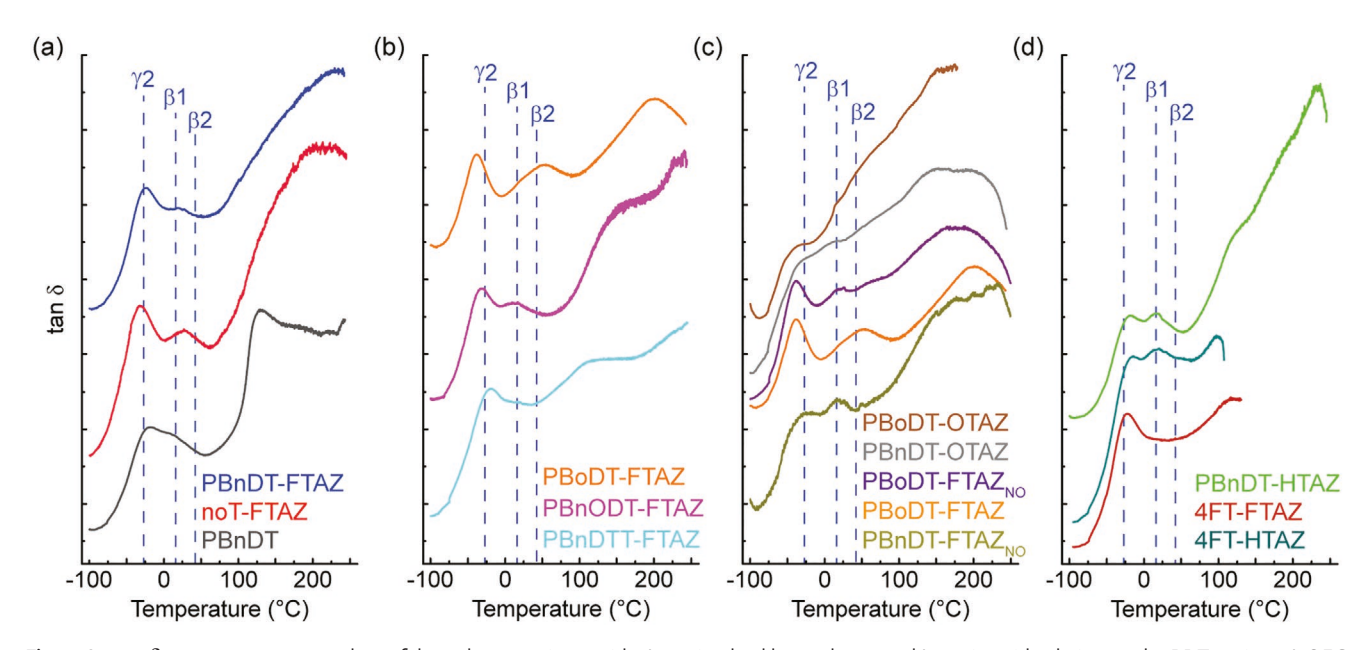


Figure 3. tan  $\delta$  versus temperature plots of the polymer variants with a) varying backbone elements, b) varying side-chains on the BDT moiety, c) OEG side-chain substitution on the BDT and the TAZ moieties, and d) fluorination along the backbone. The tan  $\delta$  curves of PBnDT-OTAZ and PBoDT-OTAZ are plotted on a semilog scale for the better visibility of the peaks. The dashed lines indicate the  $T_{\gamma 2}$ ,  $T_{\beta 1}$ , and  $T_{\beta 2}$  obtained by Gaussian fits of the PBnDT-FTAZ tan  $\delta$  curve.

through a comparison of the systematic structural variation, a number of insights into the polymer relaxation behavior can be established. In this section, we focus our attention first on the  $\gamma$ -relaxations followed by the  $\beta$ -relaxations.

### 2.2.1. \( \gamma \) Relaxations Are Dominated by Side Chains

To start, the substantial variation in backbone structure for PBnDT, noT-FTAZ, and PBnDT-FTAZ does not result in a

**Table 1.** Details of the polymers considered including number averaged molar mass  $(M_n)$ , dispersity, thermal transition temperatures obtained from the Gaussian fits of the tan  $\delta$  curves.

Polymer	$M_n$ [kg mol <sup>-1</sup> ]	Đ	$T_{\gamma 1}$ [°C]	$T_{\gamma 2} \ [^{\circ}C]^{a)}$	<i>Τ<sub>β</sub></i> 1 [°C]	Τ <sub>β2</sub> [°C]	<i>T</i> <sub>α¹</sub> [°C]	<i>T</i> <sub>b</sub> [°C]
PBnDT	78.4	2.5	-	-21	23	60	84	131
	77.8	2.4						
noT-FTAZ	76.8	3.1	-	-32	19	48	130	233
	71.6	3.5						
PBnDT-FTAZ	89.2	2.1	_	-24	18	43	113	235
	92.1	2.0						
PBnODT-FTAZ	83.2	2.2	_	-34	10	47	136	298
PBnDTT-FTAZ	34.2	2.1	_	-21	23	55	109	250
PBoDT-FTAZ	46.9	3.5	-	-39	7	51	110	203
PBnDT-FTAZ <sub>NO</sub>	69.0	2.2	-47	-19	21	66	132	232
PBoDT-FTAZ <sub>NO</sub>	39.3	2.6	_	-40	5	46	114	202
PBnDT-OTAZ	66.8	2.9	-46	-22	10	59	154	219
PBoDT-OTAZ	23.3	2.1	-58	-36	3	45	86	169
PBnDT-HTAZ	81.7	3.0	_	-19	16	36	116	241
	81.3	3.2						
4FT-HTAZ	32.4	2.3	-	-26	16	48	120	-
4FT-FTAZ	21.6	2.4	_	-21	16	46	101	_

a)The  $\gamma$ transition peaks of the polymers that are fitted with only one Gaussian fit are denoted as  $\gamma_2$ .

www.afm-journal.de

drastic change in the observed  $T_{\nu}$ . The relatively similar relaxations for the distinct difference in the backbone suggest that the side-chains are a primary driving force in the observed behavior. In fact, across a broad range of D-A-based copolymer semiconductors with alkyl side chains, a thermal relaxation is commonly observed between –40  $^{\circ}C$  and 0  $^{\circ}C.^{[5]}$  The  $T_{\sigma}$  of linear polyethylene (PE) has been found to be  $\approx$ -100 °C depending upon its MW. In branched PE, the glass transition has been found to vary from -70 to -26 °C, as measured by DSC. [43] Using the tan  $\delta$  peak to define the transition typically results in a higher measured temperature than what is measured by DSC.[43] This relaxation temperature may be further influenced by the local environment of the molecular chains. There is a drop in  $T_{\nu}$  of noT-FTAZ (-32 °C) compared to that of PBnDT-FTAZ (-24 °C) which is likely due to the higher density of the side-chains occupying the space around the monomer. The shorter distance between the side chains in the case of noT-FTAZ compared to that in the thiophene linked donor and acceptor moieties (PBnDT-FTAZ) leads to increased side-chain density for a given volume. The greater side-chain branches likely lead to larger free volume resulting in a lower  $T_{\gamma 2}$ . Further, for polymer semiconductors, it has been found that the alkyl side-chain relaxation temperature increases with length largely due to increased steric hindrance. Taken together, these considerations suggest that  $T_{\gamma}$  corresponds to a local relaxation dominated by the branched PE-like side chains.

We further ascertain that the y-transition in the studied analog polymers is indeed from the side chains by studying the variants of the polymers with different side chains attached to the BDT moiety (Figure 1b). A clear shift in relaxation temperatures with variation in side-chain structure can be observed as shown in Figure 3b. Here, we found that  $T_{\nu}$  of PBnODT-FTAZ was -34 °C, down from -24 °C for PBnDT-FTAZ (Figure 4a). This drop in  $T_{\mathcal{D}}$  is associated with the higher degree of freedom of the C-O-C bond in the alkoxy side-chain compared to the C-C-C bond of the alkyl side chain as the lone electron pair on the oxygen atom provides smaller hindrance (E = 0.08 eV) to the rotation of the O-CH<sub>2</sub> bond compared to the CH<sub>2</sub>-CH<sub>2</sub> bond (E = 0.11 eV). [45]  $T_{12}$  continues to drop when replacing the alkoxy side chain with an OEG side chain in PBoDT-FTAZ  $(T_{\nu 2} = -39 \, ^{\circ}\text{C})$ . In contrast, the thiophene on the side chain in the PBnDTT-FTAZ likely frustrates the mobility of the side

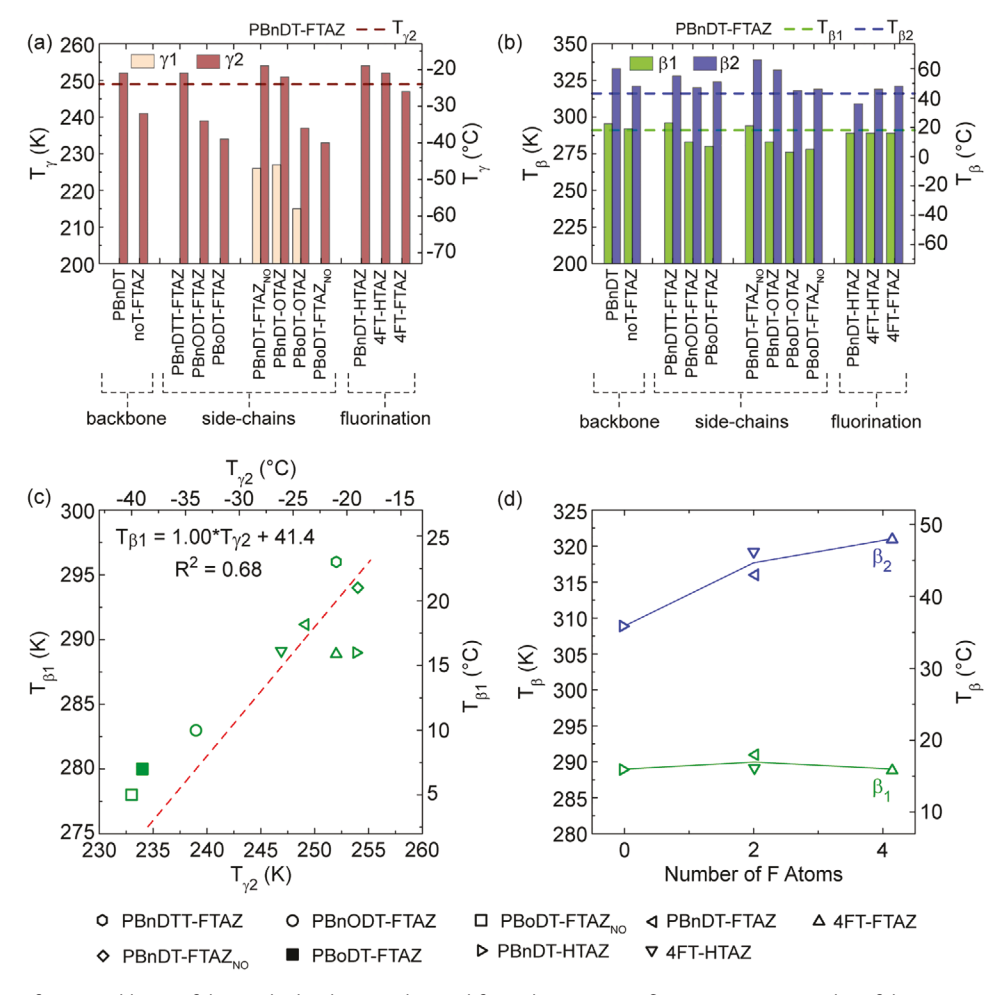


**Figure 4.** Summary of a)  $T_{\gamma}$  and b)  $T_{\beta}$  of the studied polymers obtained from the Gaussian fit. c)  $T_{\beta}$ 1 versus  $T_{\gamma 2}$  plot of the D–A variants with the fluorinated TAZ acceptor moiety and thiophene linkers. d)  $T_{\beta}$  versus number of F atoms along the polymer backbone of PBnDT-HTAZ, PBnDT-FTAZ, 4FT-HTAZ, and 4FT-FTAZ. The  $\gamma$ transition peaks of the polymers that are fitted with only one Gaussian fit are denoted as  $\gamma_2$  because the peak is dominated by the side-chains attached to the BDT moiety.





www.afm-journal.de

chain,<sup>[28]</sup> resulting in the observed increase in  $T_{\gamma 2}$  as compared to PBnDT-FTAZ. Thus, there is a clear trend that more mobile side chains result in a drop in  $T_{\gamma 2}$ . This general trend is consistent with previous reports demonstrating the importance of side chains on the thermal behavior in D–A polymers.<sup>[5,15,16]</sup>

While the relaxation is local in nature, the relaxation is influenced by interactions with other moieties in the monomer. To illustrate this point, we compare PBnDTT-FTAZ to PTB7-Th and PBDB-T, polymers that include a BDT donor with alkythiophene side chains as shown in Figures S20 and S21 (Supporting Information). Here, we find that the PBDB-T has a similar  $T_{\nu 2}$  of -24 °C to that of PBnDTT-FTAZ (-21 °C), while PTB7-Th has a significantly higher  $T_{1/2}$  at -9 °C (Figure S33, Supporting Information).<sup>[5]</sup> The lack of the thiophene linker along the PTB7-Th backbone likely leads to interaction between the F atom on the acceptor moiety and the alkyl thiophene side chains on the donor moiety increasing the relaxation temperature. Similar to PBnDTT-FTAZ, PBDB-T also has the BDT moiety separated from the acceptor moiety with thiophene linkers limiting the interaction between the two entities resulting in a similar  $T_{\gamma 2}$ . While changes in the backbone do influence  $T_{\nu}$  (e.g., drop in  $T_{\nu}$  for noT-FTAZ), the results suggest that the side chains dominate the relaxation.

### 2.2.2. Heterogeneous Side-Chains Result in Splitting of the $\gamma$ -Transition

By replacing the alkyl side chains with OEG side chains, there is a drop in the \( \gamma\) relaxation temperature, as discussed above. However, side-chain changes to the TAZ moiety are not nearly as influential on the relaxation behavior as changes to the BDT moiety. For example, the OEG side chains on the BDT moiety (e.g., PBoDT-FTAZ, PBoDT-FTAZ<sub>NO</sub>) results in a clear drop in  $T_{\nu 2}$  (-39 °C, -47 °C) relative to PBnDT-FTAZ (-24 °C). Yet, applying an OEG side-chain to the TAZ moiety (e.g., PBnDT-FTAZ<sub>NO</sub>) does not have as large of an impact on  $T_{\gamma 2}$  (-19 °C) (Figure 4a). This suggests that the relaxation of the asymmetric TAZ side chain is weaker than the symmetric BDT side chains possibly due to occupying less volume. Second, and more importantly, it was found that when the monomer includes OEG and alkyl side chains there are two Gaussian functions required to accurately fit the relaxation, including PBnDT-FTAZ<sub>NO</sub>, PBnDT-OTAZ, and PBoDT-OTAZ, see for example Figure 2d. This is observed in all cases where an OEG side chain is placed on the TAZ moiety. The exception of the mixed side chain polymers is PBoDT-FTAZ. In this case, since the BDT moiety dominates the relaxation behavior the relaxation of the TAZ moiety (likely at a high temperature given the alkyl side chain) may be obscured. In the polymers that show two peaks, the lower temperature peak is found between -46 to -58 °C. This peak is not far from the  $T_g$  of tetraethylene glycol reported to be approximately -70 °C. [46] The similar relaxation temperature provides support that the second Gaussian function capturing  $T_{\mathcal{H}}$  is due to a relaxation associated with the OEG side chains. Note that PBoDT-FTAZ and PBoDT-FTAZ<sub>NO</sub> both have a  $T_{\gamma 2}$  that is higher than the observed  $T_{\gamma 1}$  while also having significant OEG side-chain density. In these cases, the relaxation of the OEG side chains on the PBDT unit appears to be consistently near -35 °C to -40 °C, lower than the alkyl side chain variant but higher than the observed relaxation for polymers with OEG side chains on the TAZ moiety. Thus the neighboring backbone element appears to play a role in this relaxation temperature.

### 2.2.3. The $\beta$ 1-Relaxation Is Due to Twisting of the BDT Moiety and the $\beta$ 2-Relaxation Extends along the Monomer

Taking the y-transitions to be dominated by side-chain behavior, the  $\beta$ -transitions are expected to extend to a greater molecular volume. If we consider  $T_{\beta 1}$  to be a local relaxation and look at PBnDT, the only motion the BDT monomer can demonstrate is rotation about the backbone axis (Figure 2a). While this motion does not cause conformational changes, the ability of the BnDT unit to twist provides a mechanism for mechanical relaxation. [24,47] Given the similar  $T_{\beta 1}$  for PBnDT, noT-FTAZ, and PBnDT-FTAZ (Figure 4b) suggests that the  $\beta$ 1-transition is indeed associated with the relaxation of the common BnDT unit. Furthermore, a linear correlation is observed between  $T_{\vartheta}$ and  $T_{\beta 1}$ , as observed in Figure 4c. In fact, the temperature difference between  $T_{12}$  and  $T_{\beta 1}$  is remarkably similar across polymers at approximately 41 °C resulting in a linear trend line with a slope of near unity. Thus, the molecular motions at the origin of the  $\beta_1$ -relaxation follow the relaxation of the side chains on the BnDT unit  $(T_{12})$  and have a similar energetic barrier. This relationship is consistent with the postulation that the  $\beta$ 1-relaxation is associated with the twisting of the BDT unit. It should be noted that the correlation in Figure 4c is applicable only for the D-A polymers with the FTAZ moiety separated with the thiophene linkers, providing a consistent backbone arrangement.

Polymers were then considered with fluorinated thiophene and TAZ moieties along the backbone. The role of the fluorine moiety is complex, but the many noncovalent intramolecular interactions of fluorine (F $\cdots$ S, F $\cdots$ H) are believed to play an important role in solid-state packing, including planarization of the backbone and increase charge carrier mobility.<sup>[48]</sup> Across these polymers, the relaxation temperatures were observed to shift, but only marginally. The most remarkable feature is that the amount of fluorination along the backbone is positively correlated with  $T_{\beta 2}$  while  $T_{\beta 1}$  remains largely constant, as summarized in Figure 4d. These results provide insight into the origin of these relaxation temperatures. In the polymers considered, the BnDT moiety is the only constant structure along the backbone providing additional support that the similar  $T_{\beta 1}$ is associated with twisting of the BnDT unit. The relationship between  $T_{\beta 2}$  and the number of the fluorine atoms suggests that  $T_{\beta 2}$  is associated with the relaxation of the backbone that extends beyond the BnDT unit. The stronger interactions of fluorine and its larger size relative to hydrogen may lead to structural constraints that contribute to the observed behavior. [49] It should also be noted that among the polymer variants with the monofluorinated TAZ (FTAZ) moiety, the side-chain structure also impacts  $T_{\beta 2}$ , highlighting the coupled behavior between the side chains and backbone. This is consistent with previous reports showing the impact of side chains on the backbone rigidity.[15]



www.afm-iournal.de



## 2.2.4. Increasing the Side-Chain Density Results in a Larger Drop in Storage Modulus after $\mathsf{T}_{\mathsf{B}}$

Thus far, we have focused on the temperatures of the relaxations; however, the magnitude of the relaxations is also an important consideration. We found that in considering PBnDT-OTAZ and PBoDT-OTAZ, where the two hydrogenated sites on the TAZ moieties are substituted with OEG side chains, the polymer storage modulus drops more significantly with temperature when above  $T_{\beta}$ , as shown in Figure S18 (Supporting Information). Interestingly, this occurs while the relaxation temperatures stay largely constant. This is likely due to the large increase in side-chain density resulting in a larger impact of sider chain relaxation on film properties and increased steric hindrances that prevent aggregation.

#### 2.3. The $\alpha$ -Relaxation and Polymer Aggregates

The thermal transition corresponding to the  $\alpha$ -transition is observed in various polymer semiconductors and has been associated with H-bonding, [50] rigid amorphous fraction (RAF), [51,52] and aggregates. [16] The RAF is generally believed to exist at the interface between the crystalline and mobile amorphous phase in semicrystalline polymers. The polymers considered here are all largely amorphous as indicated by the lack of a melting transition as shown in the DSC scans, and previous X-ray scattering measurements. [35] Thus, we do not consider the thermal relaxation here as a rigid amorphous fraction and come back to this designation below. Sharma et al. argued that this transition is due to the thermal relaxation in aggregates. [16] We have also previously discussed these transitions and argued

that the presence of these aggregates provides toughness to the polymer films below their secondary relaxation temperatures. However, these reports did not demonstrate definitive evidence that the  $\alpha$ -relaxation is associated with aggregates. Here, we show unambiguously that the presence of aggregates (or paracrystallites) drives the  $\alpha$ -transition. To do this, we quench the film from a high-temperature anneal to avoid aggregate formation, with the procedure illustrated in **Figure 5**a. This approach allows one to clearly study thermal transitions that originate in the amorphous fractions of the polymer and suppresses the formation of ordered aggregates. We first consider regioregular P3HT and PTB7-Th, followed by PBnDT based polymers.

Regioregular P3HT is semicrystalline and shows a glass transition ( $T_g = T_\alpha = 25$  °C) and a secondary relaxation ( $T_\beta =$ -78 °C) in addition to a peak corresponding to an RAF or aggregates  $(T_{\alpha^*} = 100 \text{ °C})^{[51]}$  and crystal melting ( $\approx 230 \text{ °C}$ ), [5] as given in Figure 5a. In the quenched P3HT there was a clear absence of the  $\alpha^*$ -transition (Figure 5a) similar to our previous observations of amorphous regiorandom P3HT.[5] This suggests that the film crystallinity was significantly reduced and there was no aggregate or RAF formation. This is to be expected as quenching the P3HT sample from a melt state will inhibit the crystal and aggregate formation. This is confirmed by measuring the UV-vis absorbance of the as-cast and quenched films. with results given in Figure 5d. In the quenched films there is a loss of the 0-0 absorbance shoulder at 605 nm and the absorbance is blue shifted indicative of complete loss of aggregates and crystals.<sup>[53]</sup> PTB7-Th, on the other hand, shows one dominant secondary thermal relaxation and an  $\alpha$ -relaxation at ≈110 °C, as given in Figure S20a (Supporting Information). [5,16] The quenched PTB7-Th specimen also shows suppression of the  $T_{\alpha}$  peak (Figure S20a, Supporting Information). Unlike

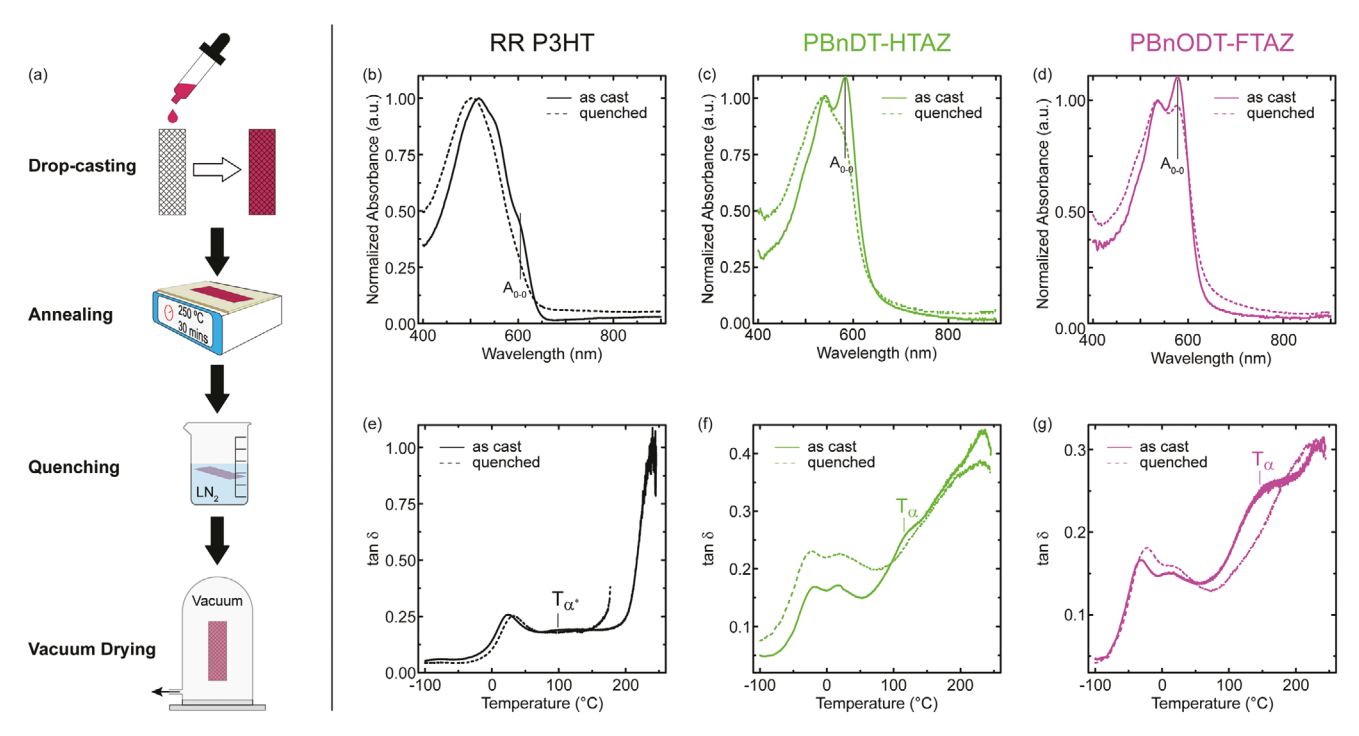


Figure 5. a) Procedure to quench aggregation in the drop-cast samples. DMA scans of as-cast and quenched samples of b) RR P3HT, c) PTB7-Th, d) PBnDT-HTAZ, and e) PBnDDT-FTAZ.  $T_{\alpha^{(k)}}$  in the case of RR P3HT indicates the aggregate relaxation temperature.





www.afm-journal.de

P3HT, PTB7-Th is an amorphous polymer as indicated by the lack of melting signature in DSC scans. [5] PTB7-Th, however, does exhibit a strong 0-0 absorbance associated with aggregates which get suppressed significantly after quenching the film from 250 °C (Figure S23a, Supporting Information). This clearly indicates that the suppression of the  $T_{\alpha}$  peak is associated with the loss of aggregates.

We apply the same approach to probe PBnDT-HTAZ, PBnDT-FTAZ, and PBnODT-FTAZ. The polymers consistently show suppression of the  $T_{\alpha}$  peak as shown in Figure 5 and Figure S23 (Supporting Information), with a corresponding loss of the 0-0 transition absorbance peak (at ≈580 nm) relative to 0-1 transition. Interestingly, quenched PBnDTT-FTAZ films do not lose the strength of the 0-0 absorbance peak as shown in Figure S23c (Supporting Information), indicating the continued presence of ordered aggregates. In this case, the DMA scans of the quenched PBnDTT-FTAZ maintain an lpha-transition peak (Figure S23f, Supporting Information), albeit weaker and at a lower temperature, resulting in a self-consistent framework. Note that in some polymers, the quenched samples show a shift in  $T_{\gamma}$  and  $T_{\beta}$  which is expected due to the competition between the formation of the ordered side chain and backbone domains.[14]

In addition, we considered in situ UV–vis spectroscopy with thermal annealing to observe how the as-cast and quenched films evolve upon heating. As shown in Figure S24 (Supporting Information), we find that as the film is heated up there is a loss in vibronic features indicative of a loss in order. We then considered deviation metric of absorbance with temperature, which was previously introduced to probe thermal relaxations, [26] with results given in Figure S24c,f (Supporting Information). In comparing the absorbance deviation of the as-cast and quenched films, we see that there is a discontinuity in the change in absorbance of the as-cast films that is not observed in the quenched films. This discontinuity is found at a temperature similar to  $T_{\alpha}$  ( $T_{\alpha^{**}}$  for P3HT) as measured by DMA, suggesting that it is indicative of a thermal relaxation event.

Taken all data together, these results provide clear evidence that the  $\alpha$ -relaxation is related to ordered aggregates (or paracrystallites) in the polymer. The quenched DMA results also reinforce the lack of a glass transition observed in the D-A copolymers. If  $T_{\alpha}$  were a glass transition, the relaxation would not diminish as observed in the quenched samples. The studied D-A copolymer samples do not completely lose their strength above  $T_{\alpha}$  possibly due to the presence of a small fraction of aggregates or crystallites that are not relaxed or melted during the high temperature anneal, which is consistent with the vibronic structure that remains visible in the quenched samples. It is important to note that we find clear similarities in the  $\alpha^*$ -relaxation in P3HT and the  $\alpha$ -relaxation of the PBnDTbased polymers. It can be argued that in P3HT, we are losing both crystallinity and associated RAF in the quenched samples, and  $T_{\alpha^*}$  is due to the relaxation of the RAF. [40,51,52] Given the common relaxation behavior between P3HT and the PBnDT variants suggests a common physical phenomenon. While the relaxation has been attributed to RAF in P3HT, the weakly crystalline nature of the PBnDT polymers leads us to ascribe the feature as aggregates. However, the ordered domains (aggregates) may not be vastly different than RAF where the polymer chains are likely more ordered given the packing constraint by the neighboring crystal.

### 2.4. Thermal Transitions and Cyclic Deformability

The fundamental thermomechanical behavior provides important insights into the stress-strain behavior of the conjugated polymers. In our previous work, we have demonstrated that the toughness of the polymer films is impacted by  $T_{\nu}$  and aggregation of the polymer chains.<sup>[5]</sup> Here we consider the stress–strain results of PBnDT-FTAZ, PBnDT-HTAZ, and PBnODT-FTAZ. To start, we measured the stress-strain response of thin films in a -pseudo-free-standing configuration with the film floating on water, [54] with the results given in Figure S34 (Supporting Information). In the free-standing tensile tests, we found that all the films began to fracture near 40% strain. The three polymers have distinct yield strength and post-yield strain hardening. PBnDT-FTAZ and PBnODT-FTAZ showed softening post yielding while PBnDT-HTAZ does not. To capture the viscoelastic-plastic behavior of the polymers (including PBnDTT-FTAZ), we varied the temperature of the films during cyclic strain tests. To do this, we use the film laminated on the thin elastomer (FLOTE) approach we previously developed and illustrated in Figure 6a.[55] In this case, the polymer film is laminated to a thin elastomer and the composite is strained. The restoring force of the elastomer substrate allows for cyclic stretching while also being thin and compliant allowing for the mechanical behavior of the polymer semiconductor to be captured. [55] The FLOTE composites were cyclically strained in the DMA from 0% to 60% at -20 °C, 0 °C, 30 °C, 70 °C, 125 °C, and 150 °C. A new sample was used for each temperature strain cycle. The temperature range was chosen such that the stretchability of the films could be studied through the  $\gamma$ ,  $\beta$ -, and  $\alpha$ -transitions. The stress–strain curves of PBnDT-FTAZ. PBnDT-HTAZ, PBnODT-FTAZ, and PBnDTT-FTAZ FLOTE composites at different temperatures are given in Figure 6b and Figure S35 (Supporting Information).

All four FLOTE composites exhibit a decrease in stiffness and residual strain (permanent set) with an increase in temperature. The drop in the extracted Young's modulus in the FLOTE tests is consistent with the magnitude of the drop in storage modulus from the DMA measurements, as compared in Figure 6c,d. As shown in Figure 6e, hysteresis under cyclic loading also decreases with temperature. The hysteresis of the composite is dominated by the polymer film as the contribution of PDMS is negligible. This hysteresis behavior is associated with energy dissipation during the deformation process and is due in part to the irreversible deformation of the polymer. The drop in hysteresis is consistent with the drop in storage modulus and the increase in relative viscous flow behavior as indicated by the increase in tan  $\delta^{[55,56]}$  While there is a drop in hysteresis with temperature there is not a distinct change in behavior across the aggregate relaxation temperature  $T_{cc}$ This may be due to the deformation behavior being dominated by the more amorphous polymer as previously observed in strained P3HT films, [55] or the relatively weak  $\alpha$ -transition. It is also important to note that all PBnDT-FTAZ samples were above its  $T_{\nu}$  resulting in a lower Young's modulus and hysteresis www.advancedsciencenews.com www.afm-journal.de

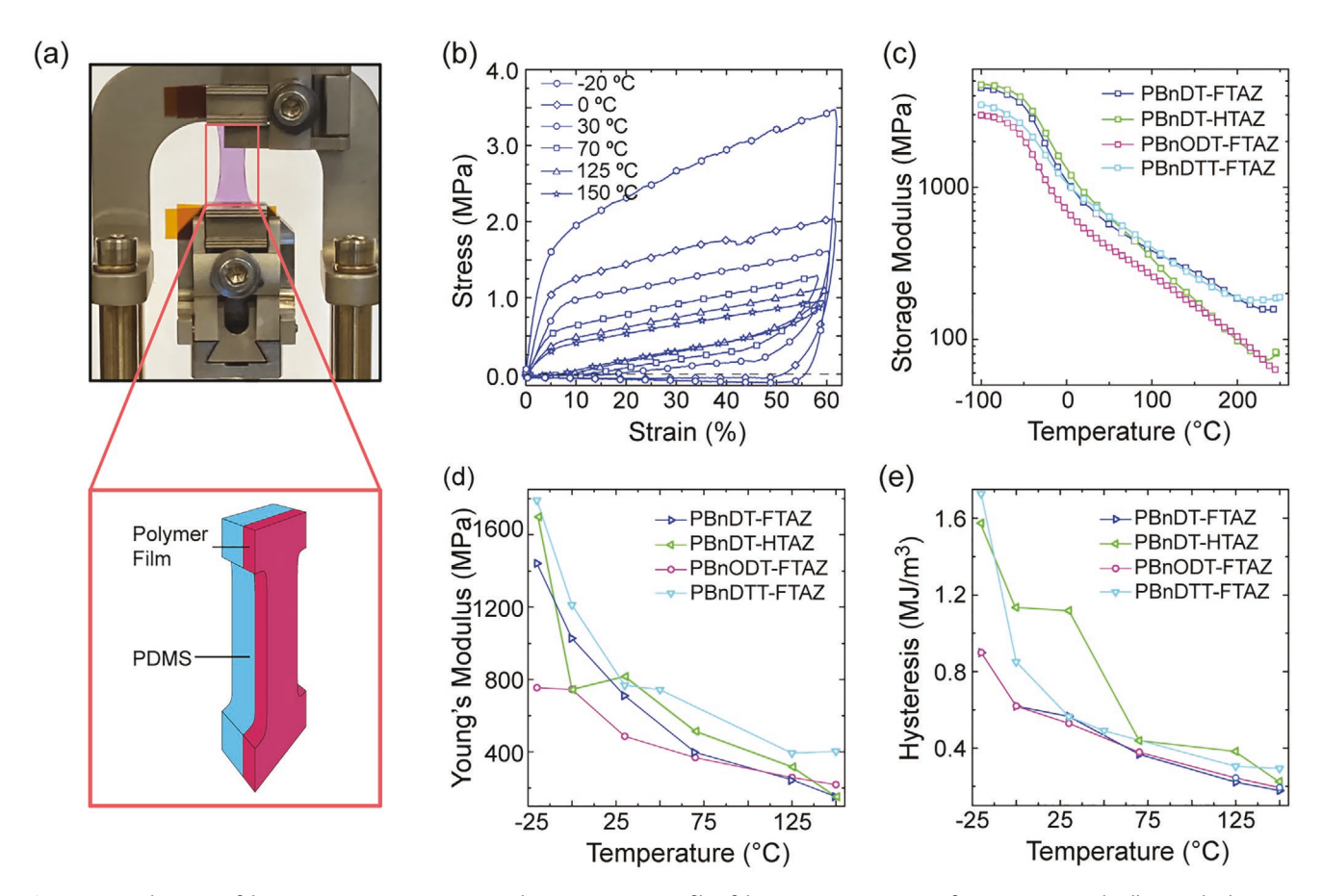


**Figure 6.** a) Schematic of the FLOTE measurement setup. b) Stress–strain profile of the FLOTE composites of PBnDT-FTAZ cyclically stretched to 60% strain at different temperatures. c) Storage modulus versus temperature profiles scaled to Young's modulus of the polymer films at 30°C extracted from the FLOTE composites. d) Young's modulus versus temperature profiles of the polymer films extracted from the FLOTE specimens. e) Hysteresis obtained from cyclic stretching of the polymer films at different temperatures.

(at -20 °C) than the other polymers. This also highlights the importance of the side-chain relaxation on cyclic stretchability of the polymer films. In all, the thermomechanical behavior under low applied strain is well correlated with the stress-strain behavior of the films. One implication of these results is that it suggests that the stronger relaxation achieved when increasing side-chain density may be a strategy to design effective stretchable polymer semiconductors as the relaxed side-chain nanodomains allow for the rigid polymer backbones to easily slide past one another, consistent with some stretchable organic device demonstrations. [57] Future research is needed to establish constitutive models that are able to capture the stress-strain behavior of the film using the viscoelastic material properties.

### 3. Conclusion

The thermal relaxations in a series of PBnDT donor and TAZ acceptor polymers with systematic variations to the backbone and side-chain chemistry were reported. Gaussian functions were fit to the tan  $\delta$  data to provide insights into the observed behavior. Through a series of observed changes in relaxation behavior, several conclusions can be drawn on the molecular origin of the relaxation event, as summarized in **Table 2**. It can

be concluded that the y-relaxations are local in nature and primarily associated with side-chain relaxations. The most striking evidence is the ability to resolve two relaxation events in the polymers with heterogeneous side chains along with the monomer. Further, thermal transitions associated with the polymer backbone ( $\beta$ -relaxations) are also observed which are local in nature. Here, the  $\beta$ 1-relaxation is found to be associated with the BnDT unit, while the closely coupled  $\beta$ 2-relaxation extends along with the monomer (at the least). The \( \gamma \)relaxations are most prominent and represent the largest drop in storage modulus, which is attributed to the large volume occupied by the side chains in these materials. Indeed, we see that as the side-chain density of these polymers was increased there was a greater drop in storage modulus after the  $\gamma$  and  $\beta$ -relaxations. All polymers considered also show a higher temperature  $\alpha$ -relaxation. We show that this transition can be suppressed by quenching the polymers from the melt. By comparing with UV-vis spectroscopy, we find that this relaxation is associated with the formation of ordered aggregates (or paracrystallites). The quenched film relaxation behavior also supports the view that the thermal relaxations observed are not a glass transition. While the results provide strong evidence on the molecular origin of the relaxation behavior. Additional complementary measurements that can probe molecular mobility, such as neutron scattering and

ADVANCED FUNCTIONAL MATERIALS

Table 2. Summary of observations from the DMA measurements.

Relaxation	Observation	Figures		
$T_{\gamma}$ $T_{\beta}$	Similar $\gamma$ and $eta$ relaxation temperatures for distinct polymers	Figure 3		
$T_{\gamma 2}$	More mobile side-chains lowers $T_\gamma$	Figures 3b and 4a		
$T_{\gamma 1}, T_{\gamma 2}$	Heterogeneous side chains results in two distinct $\gamma$ relaxations	Figures 3c and 4a		
$T_{\gamma}$ , $T_{\beta}$	Side-chain backbone interactions impact $T_\gamma$ and $T_eta$	Figures S17 and S18 (Supporting Information		
$T_{\gamma}$ , $T_{\beta}$	Increasing the side-chain density results in larger drop in storage modulus	Figure S15 (Supportin Information)		
	<b>Conclusion</b> : $T_{\gamma}$ is a local relaxation that is relaxation of the side chains			
$T_{\beta 1}$	$T_{\beta 1}$ relaxation is consistently $\approx$ 41 °C above $T_{\gamma 2}$ for a range of polymers	Figure 4c		
$T_{eta}$	$T_{eta 1}$ is constant with fluorination of the thiophene and TAZ moieties along the backbone	Figure 4d		
$T_{eta 2}$	Relaxation temperature increased with increased fluorination along the backbone	Figure 4d		
	usion: $T_{eta}$ is a local relaxation where $T_{eta 1}$ is sting of the BDT unit and $T_{eta 2}$ extends beyo			
$T_{\alpha}$	Relaxation can be reduced through quenching the films to limit aggregate formation	Figure 5		
Conclusi	on: $T_{\alpha}$ is due to relaxation of ordered aggrand no $T_{g}$ is observed.	regates in the polymer		

IR spectroscopy, will reinforce the proposed relaxation processes. Nevertheless, the results demonstrate the complex relaxation behavior observed in D-A based conjugated copolymers and make the case that the polymers do not exhibit a glass transition and the observed transitions are largely local relaxations followed by the relaxation of aggregates. We further demonstrated that the mechanical behavior of the thin films under large cyclic stretching is correlated with observed thermal relaxations. Here, we find a clear relationship between the hysteresis of the polymer under cyclic strain and the drop in storage modulus as the temperature of the sample is increased. These results illustrate the importance of understanding the thermal relaxation behavior in conjugated polymers for the development of stretchable electronics, and point to the use of large side-chain densities or more mobile side chains to improve stretchability. By increasing side-chain mobility there is a larger drop in storage modulus of the polymers with temperature and lower hysteresis under cyclic strain. Establishing the structural origins of thermal relaxations will guide not only stretchable polymer semiconductors but also the mechanical and morphological stability of all organic electronics devices.

### 4. Experimental Section

Materials: Thirteen CPs that including the BDT moiety were synthesized using microwave-assisted Stille-polycondensation

approach as shown in Scheme S1 (Supporting Information). A summary of the polymers produced and how these structural differences are organized is given in Figure 1. Details of the monomer and polymer synthesis procedure are provided in Supporting Information. Molecular weight and dispersity (*D*) of the selected polymers are provided in Table 1.

Thermal Relaxation Measurements: Thermal relaxations of the polymers were studied using a TA Instruments DMA 850. The polymer solution was drop-cast onto a glass mesh with a detailed procedure provided elsewhere. [15,18] Temperature scans were run at the oscillation frequency of 1 Hz, the oscillating strain of 0.1%, and the temperature ramp of 3 °C min<sup>-1</sup>. Peaks in tan  $\delta$  curves were identified as thermal transition temperatures unless otherwise specified and summarized in Table 1. Before running the temperature sweep, the drop-cast sample was heated to 100 °C and then cooled to -110 °C at the rate of about 30 °C min<sup>-1</sup>. This ensures the removal of solvent, moisture, and stresses within the film. The quenched films were prepared by drop-casting films and then annealing at 250 °C for 30 min to ensure that the aggregates were completely melted.<sup>[16]</sup> The samples were then immediately dipped into a liquid nitrogen bath to quench the film morphology and prevent the formation of aggregates. The samples were then left under vacuum overnight to dry without the incursion of

Film on Elastomer Measurements: A poly(4-styrene sulfonic acid) (PSS, Sigma-Aldrich) film was prepared by spin-coating the solution (1% by weight of PSS in DI water) on clean glass substrates at 5000 rpm for 30 s followed by annealing at 150 °C for 5 min. The polymer films were then spin-coated following the recipe described in Table S1 (Supporting Information). The films were then water transferred on a 500  $\mu$ m thick poly(dimethylsiloxane) (PDMS, Sylgard 184, Dow Corning) (elastomer to curing agent ratio—15:1). Crack onset strain (COS) and elastic modulus ( $E_f$ ) of the polymer films were measured using the film on elastomer (FOE) approach as discussed previously. [15,58]

Film Laminated on Thin Elastomer (FLOTE) Measurements: A thin PDMS film of a thickness ≈4 μm was prepared by spin-coating the base-curing agent mixture (15:1) in hexane (concentration of 280 mg mL<sup>-1</sup>) at 1000–1500 RPM on a PSS coated glass substrate, followed by annealing at 150 °C for 1 h. The PDMS film, patterned in a dog-bone shape, is transferred onto a thick PDMS slab. A polymer film spin-coated on a PSS coated glass substrate (Table S2, Supporting Information) is laminated on the PDMS film. The bilayer composite is then picked up and loaded in the DMA. The process is described in more detail elsewhere. [55]

UV-Vis Spectroscopy: The polymer films were spin-coated on glass substrates following the recipes in Table S2 (Supporting Information). The absorbance spectra were acquired using the Jazz UV-vis spectrometer (Ocean Optics). The quenched samples were prepared by following the protocol shown in Figure 5a. The in situ absorbance measurements were conducted using a custom-built setup using the STC 200E temperature controller (Instec Inc.), under vacuum. The deviation metric (DM<sub>T</sub>) was calculated using the equation  $DM_T = \sum_{i}^{\lambda_{max}} [I_{RT}(\lambda) - I_T(\lambda)]^2.$ 

Film on Water (FOW) Measurements: The approach to conduct tensile tests of neat polymers has been discussed in detail elsewhere. [5,56] A polymer film was spin-coated on PSS coated glass substrate. The film was cut into a dogbone shape using a  $CO_2$  laser. The polymer film was then floated on water by dissolving the PSS layer and attached to a custom-built tensile tester using PDMS grips. The film was strained at the strain rate of 1%/s using a linear translation stage (DDSM 100, Thor Labs) and the load was measured using a load cell (LVS-20GA, Kyowa). The system was controlled using a LabView program to acquire the displacement and load simultaneously.

### **Supporting Information**

Supporting Information is available from the Wiley Online Library or from the author.



www.afm-iournal.de



### Acknowledgements

N.B., S.S., and B.T.O. gratefully acknowledge support for this research through NSF CAREER award 1554322. R.S. and B.T.O. acknowledge the support of NSF award 1728370. J.J.R., H.A., and W.Y. acknowledge the support of NSF award 1639429 and NSF award 1934374. The authors thank Dr. Tingxing Zhao and Dr. Feng He (Department of Chemistry, Southern University of Science and Technology) for help with the HT-GPC measurement. The authors thank the University of North Carolina's Department of Chemistry NMR Core Laboratory for the use of their NMR spectrometers, which in part are supported by the National Science Foundations under Grant No CHE-1828183.

### **Conflict of Interest**

The authors declare no conflict of interest.

### **Data Availability Statement**

The data that support the findings of this study are available from the corresponding author upon reasonable request.

### **Keywords**

dynamic mechanical analysis, glass transition, mechanical stability, polymer semiconductors, thermomechanical relaxation

Received: June 10, 2021 Revised: August 9, 2021 Published online: October 8, 2021

- [1] S. Wu, Polym. Eng. Sci. 1990, 30, 753.
- [2] R. F. Boyer, Rubber Chem. Technol. 1963, 36, 1303.
- [3] O. Awartani, B. I. Lemanski, H. W. Ro, L. J. Richter, D. M. De Longchamp, B. T. O'Connor, D. M. DeLongchamp, B. T. O'Connor, Adv. Energy Mater. 2013, 3, 399.
- [4] N. Balar, B. T. O'Connor, Macromolecules 2017, 50, 8611.
- [5] N. Balar, S. Siddika, S. Kashani, Z. Peng, J. J. Rech, L. Ye, W. You, H. Ade, B. T. O'Connor, *Chem. Mater.* 2020, 32, 6540.
- [6] C. Müller, Chem. Mater. 2015, 27, 2740.
- [7] M. Ghasemi, H. Hu, Z. Peng, J. J. Rech, I. Angunawela, J. H. Carpenter, S. J. Stuard, A. Wadsworth, I. McCulloch, W. You, H. Ade, Joule 2019, 3, 1328.
- [8] M. Ghasemi, N. Balar, Z. Peng, H. Hu, Y. Qin, T. Kim, J. J. J. Rech, M. Bidwell, W. Mask, I. McCulloch, W. You, A. Amassian, C. Risko, B. T. B. T. O'Connor, H. Ade, *Nat. Mater.* 2021, 20, 525.
- [9] S. Himmelberger, A. Salleo, MRS Commun. 2015, 5, 383.
- [10] Q. Liu, Y. Jiang, K. Jin, J. Qin, J. Xu, W. Li, J. Xiong, J. Liu, Z. Xiao, K. Sun, S. Yang, X. Zhang, L. Ding, Sci. Bull. 2020, 65, 272.
- [11] M. S. Vezie, S. Few, I. Meager, G. Pieridou, B. Dörling, R. S. Ashraf, A. R. Goñi, H. Bronstein, I. McCulloch, S. C. Hayes, M. Campoy-Quiles, J. Nelson, *Nat. Mater.* 2016, 15, 746.
- [12] B. C. Schroeder, Y.-C. C. Chiu, X. Gu, Y. Zhou, J. Xu, J. Lopez, C. Lu, M. F. Toney, Z. Bao, Adv. Electron. Mater. 2016, 2, 1600104.
- [13] D. M. DeLongchamp, R. J. Kline, Y. Jung, E. K. Lin, D. A. Fischer, D. J. Gundlach, S. K. Cotts, A. J. Moad, L. J. Richter, M. F. Toney, M. Heeney, I. McCulloch, *Macromolecules* 2008, 41, 5709.
- [14] J. H. Carpenter, M. Ghasemi, E. Gann, I. Angunawela, S. J. Stuard, J. J. Rech, E. Ritchie, B. T. O'Connor, J. Atkin, W. You, D. M. DeLongchamp, H. Ade, Adv. Funct. Mater. 2019, 29, 1806977.

- [15] N. Balar, J. J. Rech, R. Henry, L. Ye, H. Ade, W. You, B. T. O'Connor, Chem. Mater. 2019, 31, 5124.
- [16] A. Sharma, X. Pan, J. M. Bjuggren, D. Gedefaw, X. Xu, R. Kroon, E. Wang, J. A. Campbell, D. A. Lewis, M. R. Andersson, *Chem. Mater.* 2019, 31, 6740.
- [17] S. Zhang, M. U. Ocheje, L. Huang, L. Galuska, Z. Cao, S. Luo, Y. H. Cheng, D. Ehlenberg, R. B. Goodman, D. Zhou, Y. Liu, Y. C. Chiu, J. D. Azoulay, S. Rondeau-Gagné, X. Gu, S. Rondeau-Gagné, X. Gu, Adv. Electron. Mater. 2019, 5, 1800899.
- [18] A. Sharma, X. Pan, J. A. Campbell, M. R. Andersson, D. A. Lewis, Macromolecules 2017, 50, 3347.
- [19] S. Pankaj, E. Hempel, M. Beiner, Macromolecules 2009, 42, 716.
- [20] R. Xie, A. R. Weisen, Y. Lee, M. A. Aplan, A. M. Fenton, A. E. Masucci, F. Kempe, M. Sommer, C. W. Pester, R. H. Colby, E. D. Gomez, Nat. Commun. 2020, 11, 4.
- [21] M. Xiao, A. Sadhanala, M. Abdi-Jalebi, T. H. Thomas, X. Ren, T. Zhang, H. Chen, R. L. Carey, Q. Wang, S. P. Senanayak, C. Jellett, A. Onwubiko, M. Moser, H. Liao, W. Yue, I. McCulloch, M. Nikolka, H. Sirringhaus, Adv. Funct. Mater. 2020, 31, 2007359.
- [22] S. Zhang, A. Alesadi, M. Selivanova, Z. Cao, Z. Qian, S. Luo, L. Galuska, C. Teh, M. U. Ocheje, G. T. Mason, P. B. J. St. Onge, D. Zhou, S. Rondeau-Gagné, W. Xia, X. Gu, Adv. Funct. Mater. 2020, 30, 2002221.
- [23] P. Zhan, W. Zhang, I. E. Jacobs, D. M. Nisson, R. Xie, A. R. Weissen, R. H. Colby, A. J. Moulé, S. T. Milner, J. K. Maranas, E. D. Gomez, J. Polym. Sci., Part B: Polym. Phys. 2018, 56, 1193.
- [24] S. Matsuoka, Relaxation Phenomena in Polymers, Hanser Publishers, Cincinnati, OH 1992.
- [25] K. P. Menard, Dynamic Mechanical Analysis: A Practical Introduction, CRC Press, Boca Raton, FL 2008.
- [26] S. E. Root, M. A. Alkhadra, D. Rodriquez, A. D. Printz, D. J. Lipomi, Chem. Mater. 2017, 29, 2646.
- [27] H. Pan, Y. Li, Y. Wu, P. Liu, B. S. Ong, S. Zhu, G. Xu, J. Am. Chem. Soc. 2007, 129, 4112.
- [28] H. Yao, L. Ye, H. Zhang, S. Li, S. Zhang, J. Hou, Chem. Rev. 2016, 116, 7397.
- [29] Y. Cui, H. Yao, J. Zhang, T. Zhang, Y. Wang, L. Hong, K. Xian, B. Xu, S. Zhang, J. Peng, Z. Wei, F. Gao, J. Hou, Nat. Commun. 2019, 10, 2515.
- [30] D. He, F. Zhao, J. Xin, J. J. Rech, Z. Wei, W. Ma, W. You, B. Li, L. Jiang, Y. Li, C. Wang, Adv. Energy Mater. 2018, 8, 1802050.
- [31] C. H. Y. Ho, T. Kim, Y. Xiong, Y. Firdaus, X. Yi, Q. Dong, J. J. Rech, A. Gadisa, R. Booth, B. T. O'Connor, A. Amassian, H. Ade, W. You, T. D. Anthopoulos, F. So, Adv. Energy Mater. 2020, 10, 2000823.
- [32] T. Sun, R. Song, N. Balar, P. Sen, R. J. Kline, B. T. O'Connor, ACS Appl. Mater. Interfaces 2019, 11, 3280.
- [33] N. Balar, Y. Xiong, L. Ye, S. Li, D. Nevola, D. B. Dougherty, J. Hou, H. Ade, B. T. O'Connor, ACS Appl. Mater. Interfaces 2017, 9, 43886.
- [34] Y. Huang, X. Guo, F. Liu, L. Huo, Y. Chen, T. P. Russell, C. C. Han, Y. Li, J. Hou, Adv. Mater. 2012, 24, 3383.
- [35] S. C. Price, A. C. Stuart, L. G. Yang, H. X. Zhou, W. You, J. Am. Chem. Soc. 2011, 133, 4625.
- [36] Z. Chen, L. Yan, J. J. Rech, J. Hu, Q. Zhang, W. You, ACS Appl. Polym. Mater. 2019, 1, 804.
- [37] Q. Zhang, L. Yan, X. Jiao, Z. Peng, S. Liu, J. J. Rech, E. Klump, H. Ade, F. So, W. You, Chem. Mater. 2017, 29, 5990.
- [38] N. Bauer, Q. Zhang, J. J. Rech, S. Dai, Z. Peng, H. Ade, J. Wang, X. Zhan, W. You, *Nano Res.* 2019, 12, 2400.
- [39] R. H. Boyd, Macromolecules 1984, 17, 903.
- [40] J. Martín, N. Stingelin, D. Cangialosi, J. Phys. Chem. Lett. 2018, 9, 990.
- [41] V. Di Noto, R. Gliubizzi, E. Negro, G. Pace, J. Phys. Chem. B 2006, 110, 24972.
- [42] S. Cerri, M. A. Bohn, K. Menke, L. Galfetti, Propellants, Explos., Pyrotech. 2013, 38, 190.
- [43] X. Luo, S. Xie, J. Liu, H. Hu, J. Jiang, W. Huang, H. Gao, D. Zhou, Z. Lü, D. Yan, *Polym. Chem.* **2014**, *5*, 1305.



www.advancedsciencenews.com www.afm-journal.de

ADVANCED FUNCTIONAL MATERIALS

- [44] S. A. Chen, J. M. Ni, Macromolecules 1992, 25, 6081.
- [45] B. Meng, H. Song, X. Chen, Z. Xie, J. Liu, L. Wang, *Macromolecules* 2015, 48, 4357.
- [46] J. A. Faucher, J. V. Koleske, E. R. Santee, J. J. Stratta, C. W. Wilson, J. Appl. Phys. 1966, 37, 3962.
- [47] J. Y. Jho, A. F. Yee, Macromolecules 1991, 24, 1905.
- [48] H. Huang, L. Yang, A. Facchetti, T. J. Marks, Chem. Rev. 2017, 117, 10291.
- [49] S. C. Price, A. C. Stuart, L. Yang, H. Zhou, W. You, J. Am. Chem. Soc. 2011, 133, 4625.
- [50] A. Gasperini, G.-J. N. J. N. Wang, F. Molina-Lopez, H.-C. C. Wu, J. Lopez, J. Xu, S. Luo, D. Zhou, G. Xue, J. B.-H. Tok, Z. Bao, Macromolecules 2019, 52, 2476.
- [51] N. P. Holmes, M. Marks, J. M. Cave, K. Feron, M. G. Barr, A. Fahy, A. Sharma, X. Pan, D. A. L. Kilcoyne, X. Zhou, D. A. Lewis, M. R. Andersson, J. van Stam, A. B. Walker, E. Moons, W. J. Belcher, P. C. Dastoor, *Chem. Mater.* 2018, 30, 6521.

- [52] S. Luo, T. Wang, M. U. Ocheje, S. Zhang, J. Xu, Z. Qian, X. Gu, G. Xue, S. Rondeau-Gagné, J. Jiang, W. Hu, E. Zhuravlev, D. Zhou, *Macromolecules* 2020, 53, 4480.
- [53] J. Clark, C. Silva, R. H. Friend, F. C. Spano, Phys. Rev. Lett. 2007, 98, 206406.
- [54] J.-H. Kim, A. Nizami, Y. Hwangbo, B. Jang, H.-J. Lee, C.-S. Woo, S. Hyun, T.-S. Kim, *Nat. Commun.* 2013, 4, 3283.
- [55] R. Song, H. Schrickx, N. Balar, S. Siddika, N. Sheikh, B. T. O'Connor, B. T. O'Connor, Macromolecules 2020, 53, 1988.
- [56] A. D. Drozdov, R. Klitkou, J. D. Christiansen, Mech. Mater. 2013, 56, 53.
- [57] C. Lu, W.-Y. Y. Lee, X. Gu, J. Xu, H.-H. H. Chou, H. Yan, Y.-C. C. Chiu, M. He, J. R. Matthews, W. Niu, J. B. H. B.-H. Tok, M. F. Toney, W.-C. C. Chen, Z. Bao, Adv. Electron. Mater. 2017, 3, 1600311.
- [58] C. M. Stafford, C. Harrison, K. L. Beers, A. Karim, E. J. Amis, M. R. VanLandingham, H. C. Kim, W. Volksen, R. D. Miller, E. E. Simonyi, *Nat. Mater.* 2004, 3, 545.